Meniscus ECM functionalized hydrogels containing infrapatellar fat pad derived stem cells for bioprinting of regionally defined meniscal tissue

S.Romanazzo[1,2,5], S.Vedicherla[1,3], C. Moran[1,2,3], D.J. Kelly[1,2,4,5]*

[1] Trinity Centre for Bioengineering, Trinity Biomedical Science Institute, Trinity College Dublin, Ireland

[2] Advanced Materials and Bioengineering Research (AMBER), Trinity College Dublin, Ireland

[3] Orthopaedics and Sports Medicine, School of Medicine, Trinity College Dublin, Ireland

[4] Department of Anatomy, Royal College of Surgeons in Ireland, Dublin, Ireland

[5] Dept of Mechanical and Manufacturing Engineering, School of Engineering, Trinity College Dublin, Ireland

* Corresponding author

Prof. Daniel J. Kelly

Director - Trinity Centre for Bioengineering

Email address: kellyd9@tcd.ie

Telephone: 353-1-8963947

Fax 353-1-6795554

Address: Dept of Mechanical and Manufacturing Engineering, School of Engineering, Trinity College Dublin, Ireland.

Key words

Meniscus, stem cell, 3D bioprinting, hydrogels, PCL, scaffolds, CTGF, TGFβ3

Abstract

Injuries to the meniscus of the knee commonly lead to osteoarthritis. Current therapies for meniscus regeneration, including meniscetomies and scaffold implantation, fail to achieve complete functional regeneration of the tissue. This has led to increased interest in cell and gene therapies and tissue engineering approaches to meniscus regeneration. The implantation of a biomimetic implant, incorporating cells, growth factors and extracellular matrix (ECM) derived proteins, represents a promising approach to functional meniscus regeneration. The objective of this study was to develop a range of ECM functionalised bioinks suitable for 3D bioprinting of meniscal tissue. To this end, alginate hydrogels were functionalised with ECM derived from the inner and outer regions of the meniscus and loaded with infrapatellar fat pad derived stem cells (FPSCs). In the absence of exogenously supplied growth factors, inner meniscus ECM promoted chondrogenesis of FPSCs, while outer meniscus ECM promoted a more elongated cell morphology and the development of a more fibroblastic phenotype. With exogenous growth factors supplementation, a more fibrogenic phenotype was observed in outer ECM functionalised hydrogels supplemented with CTGF, while inner ECM functionalised hydrogels supplemented with TGFβ3 supported the highest levels of Sox-9 and type II collagen gene expression and sGAG deposition. The final phase of the study demonstrated the printability of these ECM functionalised hydrogels, demonstrating that their co-deposition with PCL micro-fibres dramatically improved the mechanical properties of the 3D bioprinted constructs with no noticeable loss in cell viability. These bioprinted constructs represent an exciting new approach to tissue engineering of functional meniscal grafts.

1. Introduction

Approximately 1.5 million meniscal surgeries are performed across the United States and Europe annually and are among the most common procedures performed by orthopaedic surgeons (Parker et al., 2016; OECD/EU, 2016). Following a meniscectomy, consisting of the surgical removal of all or part of damaged meniscus tissue, the intrinsic regeneration capacity remains poor, especially when a wide area of the tissue is resected. In addition, although partial meniscectomies often relieve symptoms in the short term, long-term follow-up indicates that meniscal removal leads to an increased risk of osteoarthritis, which may be explained by the fact that such a substantial loss of meniscal tissue alters the biomechanical and biological environment of the joint (Antony et al., 2016). No intervention (*i.e.* meniscectomy, intra-articular cell delivery, gene-therapy) has been developed to facilitate true regeneration of an injured meniscus (Moran et al., 2015; Scotti et al., 2013). Organ transplantation remains the only efficient remedy for serious meniscus damage, however this approach is impeded by donor availability, concerns associated with disease transmission and limited remodelling of the allograft into a living, functional tissue (Steadman and Rodkey, 2017). This has led to increased interest in meniscal tissue engineering strategies, although the optimal combination of biomaterials, cells and instructive cues to drive successful regeneration has yet to be established.

Meniscus cells, articular cells, costal and nasal chondrocytes, bone marrow mesenchymal stem cells (BMSCs), synovial membrane-derived stem cells (SDSCs) and embryonic stem cells have all been proposed as a cell source for meniscal tissue engineering (Andia and Maffulli, 2016; Yu et al., 2015). BMSCs are an attractive option, but their propensity for osteogenesis limits their use for meniscal tissue

engineering (Makris et al., 2011; Van der Bracht et al., 2007). We have demonstrated that infrapatellar fat pad derived stem cells (FPSCs) represent an attractive alternative to BMSCs for engineering of cartilaginous tissues (Vinardell et al., 2012; Buckley et al., 2010; Mesallati et al., 2015; Carroll et al., 2014; Luo et al., 2016). In terms of instructive cues, a number of growth factors (GFs), hormones and other small molecules are known to influence the development and regeneration of meniscal tissue. Of relevance, the GFs connective tissue growth factor (CTGF) and hepatocyte growth factor (HGF) have been shown to stimulate the formation of the outer meniscus region and to improve vascularization essential for a vital peripheral zone of the meniscus, while the GFs platelet derived growth factor-BB (PDGF-BB) and insulin-like growth factor-1 (IGF-1) have been shown to support development of the inner part of the meniscus (Park and Na, 2008; Lee et al., 2006). A variety of scaffolds have also been developed to provide an appropriate environment for meniscal repair (Di Matteo et al., 2015; Vrancken et al., 2013; Fisher et al., 2013, 2017; Lee et al., 2014). In recent years, there has been an increased interest in the use of natural ECM derived biomaterials to support tissue regeneration (Almeida et al.; 2016; Almeida et al., 2017; Visser et al., 2015; Wolf et al., 2012). Of relevance to meniscal regeneration, it has been shown that injectable gels derived from decellularized meniscus ECM have been shown to support cell growth, and when injected *in vivo* showed hydrogel formation and tissue compatibility (Wu et al., 2015). It has also been demonstrated that ECM from different regions of the meniscus (either the inner or outer region) can be used as a biomaterial to support region specific hMSC fibrochondrogenic differentiation (Rothrauff et al., 2016; Shimomura et al., 2016). Furthermore, it has been shown that combining electrospun fibers of polylactic

acid (PLA) with ECM derived hydrogels can be used to improve the mechanical properties of meniscal constructs (Baek et al., 2015).

In spite of these developments, such strategies have generally failed to regenerate meniscal tissue mimicking the complex spatial structure, composition and biomechanics of the native tissue. In recent years, 3D bioprinting has emerged as a promising strategy to create 3D engineered tissues that can mimic the anatomic shape of the organ of interest (Skardal and Atala, 2015; Ahn et al., 2012; Hong et al., 2015, Markstedt et al., 2015; Yang et al.,2017). Gels derived from decellularized native ECM have been proposed as bioinks, promoting high levels of cell viability and tissue specific differentiation (Pati et al., 2014). The goal of this study was to develop biomimetic constructs which can instruct encapsulated stem cells to differentiate into either meniscal chondrocytes or fibroblasts. To this end, alginate hydrogels were first functionalized with ECM isolated from either the inner and outer regions of the meniscus. To access the capacity of such constructs to support meniscal region specific tissue development, they were seeded with FPSCs and cultured in the presence or absence of TGFβ3 or CTGF. We also explored whether such ECM functionalised hydrogels can be used as bioinks for 3D bioprinting, and examined their co-deposition alongside PCL micro-filaments to fabricate mechanically reinforced constructs suitable for implantation into load bearing environments.

2. Materials and Methods

2.1. Development of alginate hydrogels functionalized with meniscus ECM

ECM was extracted from porcine menisci (2-3 months old). The outer region of the meniscus was separated from the inner region, as shown in Fig. 1A. Both regions

were minced into 1-2 mm sized pieces, digested with 30 U/mg pepsin and then freeze dried as previously described (Almeida et al., 2017). Freeze dried ECM was stored at -80 °C until usage. To prepare ECM functionalized hydrogels, ECMs were resolubilized in 0.02% acetic acid and neutralized to a pH of 7.2 - 7.4 by adding an appropriate amount of 0.1 M NaOH, in order to obtain a solution of 10 mg/mL, and incubated overnight under continuous rotation at 4 °C. Both Inner ECM and Outer ECM were then mixed together with alginate and FPSCs, according to a protocol described in Section 2.3. Decellularization of the ECMs were ensured by the absence of DAPI staining, used to counterstain cell nuclei.

2.2. Isolation and expansion of porcine fat pad derived stem cells

Knee joints were dissected from 2-3 months old pigs to harvest infrapatellar fat pad and isolate stem cells using established procedures (Buckley et al., 2010). Briefly, tissue was minced and digested with 750U/ml collagenase type II (Gibco, Biosciences, Ireland) at 10ml/g for 3-4 hours at 37 °C in serum free DMEM GlutaMAX with 100 U/ml penicillin, 100 mg/ml streptomycin (P/S) (all Gibco, Biosciences, Ireland) and amphotericin B (0.25 mg/ml) (Sigma-Aldrich, Ireland). Digested tissue suspensions were filtered through a 40μm cell strainer to remove tissue remains and washed two times by repeated centrifugation at 650 g for 5 min. Cell yield and viability was determined with a hemocytometer and trypan blue exclusion. Cells for expansion were seeded at an initial density of 5 x 10^3 cells/cm^2 in T-175 flasks in DMEM GlutaMAX supplemented with P/S and 10% fetal bovine serum (FBS) (all Gibco, Biosciences, Ireland), at 37°C and 5% CO_2. From hereafter, this media will be referred as standard culture media. When 70% confluence was reached, cells were expanded up to passage 2 and then used for the desired purpose.

2.3. Encapsulation and culture of FPSC in alginate-ECM hydrogels

FPSC at passage 2 were detached from the tissue culture plates by treatment with 0.05% trypsin/0.53 mM ethylenediaminetetraacetic acid (EDTA) (Sigma-Aldrich, Ireland) and re-suspended in standard culture media. 4% agarose cylindrical shape moulds (5 x 3 mm) containing 60 mM $CaCl_2$ (al Sigma-Aldrich, Ireland) were used to prepare cells encapsulated in alginate and alginate/ECM gels. Each gel had a seeding density of $8x10^6$ cells/mL. For gels including ECM, cells re-suspended in standard culture media were first mixed together with the appropriate amount of ECM (10 mg/mL) in order to have a final concentration of 2 mg/mL, and then 2.5% Alginate (UP LVG, Pronova, Norway) dissolved in sterile Phosphate Buffer Saline (PBS) (Sigma-Aldrich, Ireland) to obtain a final concentration of 1.1% Alginate. The entire mix was then poured into agarose/$CaCl_2$ moulds and incubated at 37°C and 5% CO_2 for 1 h, to allow ionic crosslinking of the alginate. For alginate only gels, 2.5% alginate was added to cells (8×10^6 cells/ mL) and the volume was adjusted by adding standard culture media. Following gelation each gel was removed from the mould and transferred into culture dishes and cultured for up to 21 days at 37° C, 5% CO_2 and 5% O_2 with the appropriate type of media: standard culture media, chondrogenic (supplemented with 10 ng/ml of TGFβ3 supplemented) or fibrochondrogenic (supplemented with 100 ng/ml of CTGF). Chondrogenic media consisted of DMEM GlutaMAX (Gibco, Biosciences, Ireland) supplemented with P/S, 100 µg/mL sodium pyruvate, 40 µg/mL L-proline, 50 µg/mL L-ascorbic acid 2-phosphate, 4.7 µg/mL linoleic acid, 1.5 mg/mL bovine serum albumin, 1X insulin– transferrin–selenium, 100 nM dexamethasone (all from Sigma-Aldrich, Ireland) and 10 ng/mL human TGFβ3 (Prospec-Tany TechnoGene Ltd, Israel). Alternatively cells were cultured in DMEM GlutaMAX supplemented with P/S, 10% FBS (all Gibco, Biosciences,

Ireland) and 100 ng/mL human CTGF (Prospec-Tany TechnoGene Ltd, Israel). Media exchange was performed twice weekly.

2.4. Cell viability assay, immunofluorescence staining and confocal microscopy

Cell viability was established using a live/dead assay kit (Invitrogen, Bioscience, Ireland). All constructs were rinsed in PBS and incubated for 1 h at 37°C in a solution containing 2 μM calcein, for green staining of live cells, and 4 μM of ethidium homodimer-1, a red label for dead cells. Following, samples were rinsed again and imaged with Leica SP8 Confocal Microscope at 488 nm and 543 nm wavelengths. Cell viability was then quantified using Image-J software.

For analysing cell shape, all constructs were washed in PBS and fixed with 4% paraformaldehyde (PFA) (all Sigma-Aldrich, Ireland) solution for 3 h at 10 rpm rotation. Samples were then incubated with tetra-rhodamine-conjugated Phalloidin (1:100) (Invitrogen, Bioscience, Ireland) for 1h at room temperature, to detect through immunofluorescence analysis F-actin and thus visualize cell morphology and cystoskeleton organization. For protein expression of collagen type I and collagen type II (1:100, Sigma-Aldrich, Ireland), samples were incubated 1h at room temperature and then appropriate secondary antibody anti-mouse Alexa Fluor® 488 (1:200) (eBioscience, San Diego, California, USA) was added for 1 h. Nuclei were counterstained with 4′, 6-diamidino-2-phenylindole (DAPI) (Sigma-Aldrich, Ireland). Images were taken using Leica SP8 Confocal Microscope, at 532 nm and 358 nm. The composition of the inner and outer ECM were compared to commercially available collagen type I, from rat tail (Corning Inc., NY, USA) and collagen type II, from chicken sternal cartilage (Sigma-Aldrich, Ireland).

2.5. Quantitative biochemical analysis

Biochemical content of DNA, proteoglycans (sGAG) and collagen was assessed by using n=5 constructs for each group. First, 125 μg/mL papain in 0.1 M sodium acetate, 5 mM L-cysteine-HCl, 0.05 M EDTA, pH 6 (all from Sigma-Aldrich, Ireland) was used to digest samples at 60 °C under constant rotation for 18 h. Alginate was uncrosslinked by using 1M sodium citrate solution. DNA content was determined using the Hoescht 33258 dye-based assay (DNA QF Kit, Sigma-Aldrich, Ireland) with a calf thymus DNA standard. sGAG was quantified using the dimethylmethylene blue dye-binding assay (Blyscan, Biocolor Ltd., Northern Ireland), with a chondroitin sulphate standard. Total collagen was determined by measuring the hydroxyproline content. For this purpose, samples were hydrolysed at 110 °C for 18 h in 38% HCl diluted in H_20 and assayed using a chloramine-T assay with a hydroxyproline:collagen ratio of 1:7.69. Each biochemical constituent was normalised to the tissue wet weight (%w/w) measured before sample digestion.

2.6. Quantitative RT-PCR analysis

For mRNA expression analysis of FPSC cultured under different conditions, cells were maintained in culture for the required days at 37 °C, in 5% CO2 and 5% O_2. Subsequently, FPSC encapsulated in gels were first treated with an alginate dissolving buffer, containing Sodium Citrate (55 mM), EDTA (30 mM) and NaCl (150 mM) (all Sigma-Aldrich, Ireland) for 10 min at 37 °C, and then centrifuged for 1 min at 10.000 rpm. The obtained cell pellet was then resuspended in the so called RLT buffer from the RNeasy Kit (Qiagen, Valencia, USA). An incubation of 10 min at 55 °C with Proteinase K was added to the standard RNA isolation protocol, to allow the entire dissolution of ECM components in the gels. Subsequent steps were performed

following the manufacturer's instructions (Qiagen, Valencia, USA). For FPSC cultured in culture dishes, cells were detached using 0.05% trypsin/0.53 mM EDTA (Sigma-Aldrich, Ireland) treatment and subjected to the standard RNA isolation protocol using RNeasy Kit (Qiagen, Valencia, USA). 500 ng of total RNA was reverse-transcribed into cDNA with a random hexamer primer using High-Capacity cDNA reverse transcription kit (Applied Biosystems, Biosciences, Ireland) according to the manufacturer's instructions. cDNA quality was then quantified by Qubit® dsDNA assay kit (Applied Biosystems, Biosciences, Ireland) and then RT-PCR was performed using a 7500 Fast RT-PCR (Applied Biosystems, Biosciences, Ireland). Standard reactions were prepared in 96-well plates (Micro Amp, Applied Biosystems). The reaction mixture was composed of 10 µL of SYBR Select Master Mix (Applied Biosystems, Biosciences, Ireland), 10 pmol each of the forward and reverse primers, 2 µL of cDNA and distilled water to a final volume of 20 µL. The thermocycling conditions were 95 °C for 30 s, followed by 40 cycles of 95 °C for 5 s and 60 °C for 34 s. Normalization of the data was performed using the housekeeping gene glyceraldehyde- 3-phosphate dehydrogenase (GAPDH) as an endogenous control in the same reaction as the gene of interest.

The primers used in this study were as follows: for GAPDH, forward primer 5′-TTTAACTCTGGCAAAGTGG-3′ and reverse primer 5′-GAACATGTAGACCATGTAGTG-3′; Collagen type I (COL1A1), forward primer 5'-TAGACATGTTCAGCTTTGTG-3' and reverse primer 5'-GTGGGATGTCTTCTTCTTG-3'; Collagen type II (COL2A1), forward primer 5'-CGACGACATAATCTGTGAAG-3' and reverse primer 5'-TCCTTTGGGTCCTACAATATC-3'; SRY (Sex Determining Region Y)-Box-9 (Sox9), forward primer 5'-CAGACCTTGAGGAGACTTAG-3' and reverse primer

5’-GTTCGAGTTGCCTTTAGTG-3’; Aggrecan (ACAN), forward primer 5′-GACCACTTTACTCTTGGTG-3′ and reverse primer 5′-TCAGGCTCAGAAACTTCTAC-3′; Tenascin-C (TNC), 5’-ATCTAGTCTTTCTCAACTCCG-3’ and reverse primer 5’GAGTAGAATCCAAACCAGTTG-3’. The specificity of the SYBR PCR signal was confirmed by melt curve analysis. Ct values were transformed into relative quantification data using the $2^{-\Delta\Delta Ct}$ method, and data were normalized to GAPDH mRNA expression.

2.7. Histological analysis

Samples were fixed in 4% PFA, dehydrated with a graded series of alcohol, and embedded in paraffin. 8 μm sections were produced of the cross section of construct face. sGAG deposition was assessed using Aldehyde Fuschin and 1% alcian blue 8GX in 0.1M HCL (all from Sigma-Aldrich, Ireland).

Collagen types I and II were evaluated using a standard immunohistochemical technique. Briefly, sections were rehydrated and treated with chondroitinase ABC (Sigma-Aldrich, Ireland in a humidified environment at 37 °C. Following, samples were incubated overnight at 4 °C, with a solution containing goat serum to prevent nonspecific sites binding and the relevant primary collagen type I (ab90395, 1:400) or collagen type II (ab3092, 1:100) (Abcam, UK). Treatment with peroxidase preceded the application of the secondary antibody (1.5:200) (Abcam, UK) at room temperature for 1 h. Thereafter, all sections were incubated with ABC reagent (Vectastain PK-400) (Vector Laboratories, UK) for 45 min. Finally, sections were developed with DAB peroxidase (Vector Laboratories, UK) for 5 min. Positive and negative controls were included in the immunohistochemical staining protocols. Sections were imaged

with an Olympus IX51 inverted microscope fitted with an Olympus DP70 camera.

2.8. 3D Bioprinting

The 3D bioplotter from RegenHU (3D Discovery, Switzerland) was used for printing of alginate-ECM bioinks using previously established settings (Daly et al., 2016). Polycaprolactone (PCL) with a molecular weight of 45.000 (Sigma-Aldrich, Ireland) was first melted at 70 °C in the printing chamber. A screw driven piston (25 rev/min, screw diameter 1 cm) with a 25 G Gauge needle extruded the PCL onto a coverslip at 65 °C and at a 4 MPa pressure. Bioinks were prepared by combining cells, alginate and ECM (inner or outer) and 48 mM $CaCl_2$ solution to pre-crosslink alginate before printing. Then, the entire mixed solution was loaded into the printing column and a 25 G straight needle was used to print each hydrogel at a pressure of 2 MPa. After printing, the entire construct was incubated in 92 mM $CaCl_2$ for 15 min and then transferred into a culture plate with standard culture media and kept at 37 °C and 5% CO_2 for 24 h.

2.9. Mechanical Testing

Mechanical tests were performed using a single column Zwick (Zwick, Roell, Germany) with a 100 KN load cell as previously described (Olvera et al., 2015). Briefly, stress relaxation tests were performed using impermeable metal platens. The equilibrium modulus was determined by applying a 10% unconfined compressive strain with a ramp displacement of 0.001 mm/s. A relaxation period of 30 min was used.

2.10. Statistical analysis

Statistical analyses were performed using GraphPad Prism (version 5) software with 3-5 samples analysed for each experimental group. One-way or two-way ANOVA was used for analysis of variance with Bonferroni's post-tests to compare between groups. Results are provided as mean ± standard deviation of $n \geq 3$ independent experiments. Values were considered significant when $p < 0.05$.

3. Results and Discussion

3.1. Characterization of meniscus derived ECM

ECMs were extracted from different parts of porcine menisci. The outer and inner region of each meniscus was divided, digested and decellularized (Fig. 1A). Each extracted ECM was then characterized for their collagen type I (Col. I) and collagen type II (Col. II) content and compared to commercially available collagen type I from rat tail (Corning Inc., NY, USA) and collagen type II from chicken sternal cartilage (Sigma-Aldrich, Ireland). As expected, the inner meniscus ECM stained strongly for Col. II and weakly for Col. I, while the outer region ECM stained strongly for Col. I and less intensely for Col. II (Fig. 1B). Commercially available collagen type I and II both stained positive for Col. I, but weakly for Col. II. In addition to the types of collagen present, the composition of inner and outer meniscus ECM have been shown to differ in other ways. It has been demonstrated that the inner meniscus ECM also contains higher level of proteoglycans and growth factors such as TGFβ2 and TGFβ3, while the outer meniscus ECM is rich in bFGF and insulin (Rothrauff et al., 2016). Endogenous growth factors within ECMs are believed to play a key role in determining their bioactivity (Rothrauff et al., 2017). Further work is required to completely characterise the composition of different regions of the meniscus ECM.

3.2. Meniscal ECM regulates the morphology and differentiation of joint derived stem cells in a region specific manner

To generate ECM functionalized hydrogels, alginate was either combined with either inner ECM (*IN*) or outer ECM (*OUT*). As a control, cells were cultured in alginate only hydrogels (*ALG*). As a first step, each group was analysed *in vitro* by generating FPSC laden hydrogels (5 x 3 mm) and culturing them in standard culture media for 21 days without the addition of any growth factors. FPSC morphology after 21 days was found to depend on the specific type of ECM incorporated into the hydrogel; FPSCs encapsulated within *IN* hydrogels maintained their rounded cell shape (Fig. 2A, centre), where FPSCs in the *OUT* hydrogels displaying a more mixed morphology, with a tendency towards a more elongated fibroblast-like shape (Fig. 2A, right). FPSCs maintained a rounded morphology in *ALG* controls (Figure 2A, left). To assess if these changes in cell shape correlated with differences in FPSC fibrochondrogenesis, we assessed type I and type II collagen gene expression and protein production and sGAG synthesis within the hydrogels. Type II collagen protein production (Fig. 2D) and gene expression (Fig. 2E) was higher in *IN* compared to *OUT* hydrogels. Less dramatic differences in type I collagen protein production (Fig. 2B) and gene expression (Fig. 2C) were observed between groups. While all hydrogels stained strongly for sGAG deposition (Fig. 2F), biochemical analysis revealed significant higher levels of GAG synthesis within *IN* gels (Fig. 2G). These findings demonstrated that alginate hydrogels functionalized with inner meniscus ECM can support chondrogenesis of FPSCs in the absence of exogenously supplied growth factors, while outer meniscus ECM supports the development of a more elongated cell morphology and a fibrogenic phenotype.

These findings are in agreement with previous studies which demonstrate the importance of ECM composition on stem cell differentiation (Pati et al., 2014) and in particular with recent findings that MSCs cultured in the presence of decellularized ECM obtained from either the inner or outer regions of the meniscus differentiate along chondrogenic or fibroblastic pathways respectively (Shimomura et al., 2016; Rothrauff et al., 2016). A difference between our study and earlier investigations is the hydrogel within which ECM components and cells are combined (alginate versus PEG), suggesting that ECM can exert its biological effect when encapsulated within a range of different carriers. A novel finding of the present study is that region specific meniscal ECM can differently affect cell morphology and stimulate either fibrochondrogenesis or chondrogenesis of joint derived stem cells without the addition of exogenous growth factors. This result suggests that ECM composition can influence cell adhesion and thus cell morphology, which downstream is likely modulating cell differentiation (Tan & Cooper-White 2011). The choice of using joint derived stem cells (*e.g.* FPSCs) as a cell type is also another novelty of this study, as the majority of previous strategies for meniscal tissue regeneration have focused on bone marrow as a stem cell source. FPSCs can be easily harvested during knee surgery and they have a notable capacity for self-renewal and chondrogenesis (Buckley et al., 2010; Vinardell et al., 2012).

3.3. Combining region specific ECM and growth factors to promote the development of distinct meniscal cell phenotypes

After assessing the effect of ECM in isolation on FPSC differentiation, we next explored the co-stimulation with growth factors known to specifically induce chondrogenesis (TGFβ3) or fibrochondrogenesis (CTGF) (Lee et al., 2010; Moioli and Mao, 2006). Specific concentrations of these growth factors were chosen based

on the results of previous studies exploring meniscus regeneration (Lee et al. 2014). When *OUT* hydrogels were stimulated with CTGF, FPSCs again adopted a more spread, fibroblast-like morphology (Fig. 3A, top-right), while FPSCs encapsulated within inner ECM gels maintained their round shape. (Fig. 3A, top-middle). When stimulated with TGFβ3, FPSCs within the *IN* hydrogels tended to aggregate and form clusters (Fig. 3A, bottom-middle). Less aggregation and cell clustering was observed in the *ALG* hydrogels (Fig. 3A, down-left). Higher levels of DNA content were measured in TGFβ3 stimulated hydrogels compared to CTGF stimulated hydrogels (data not shown), suggesting higher levels of FPSC proliferation in response to TGFβ3 stimulation.

Lower levels of sGAG deposition was observed in CTGF treated groups (Fig. 3C) compared to TGFβ3 treated groups (Fig. 3E). Within the CTGF treated samples, the *IN* constructs (Fig. 3C, middle) stained most intensely for sGAG deposition (Fig. 3D), with a similar trend observed in the biochemical analysis (Fig. 3B). Similarly, *IN* hydrogels stimulated with TGFβ3 contained significantly higher levels of sGAG than other groups stimulated with this growth factor (Fig. 3D). It should also be noted that absolute levels of sGAG deposition, when normalised to construct weight and not DNA, were significantly higher in all TGFβ3 stimulated constructs compared to CTGF stimulated constructs (data not shown).

Immunohistochemical analysis demonstrated robust deposition of type I collagen in all groups treated with CTGF (Fig. 4A, left column), with less intense staining observed in hydrogels stimulated with TGFβ3 (Fig. 4B, left column). Among the CTGF groups, the *OUT* hydrogels stained less intensely for type II collagen compared to the *IN* hydrogels. Overall, the strongest staining for type II collagen was observed in the *IN* hydrogels supplemented with TGFβ3. In agreement with the

immunohistochemical analysis, type I collagen was expressed at higher levels in all CTGF groups (Fig. 4C), while type II collagen expression was higher in samples treated with TGFβ3 (Fig. 4D). Among the TGFβ3 treated groups, Sox 9 and type II collagen expression was highest within the *IN* hydrogels (Fig. 4E and 4D respectively). Significantly lower levels of ACAN expression were observed in *OUT* hydrogels compared to ALG hydrogels when stimulated with either CTGF or TGFβ3 (Fig. 4F). In addition, the fibrochondrogenic marker TNC was up-regulated in samples stimulated with CTGF (Fig. 4G, left). In TGFβ3 treated samples, TNC expression was significantly higher in *OUT* compared to *IN* hydrogels. (Fig. 4G, right).

Together these results demonstrate that different ECMs can be combined with specific growth factors to differentially regulate the phenotype of FPSCs for region specific meniscus tissue engineering. This is in agreement with recent studies that demonstrated cartilage ECM incorporated into a GelMA hydrogel enhanced chondrogenesis of encapsulated MSCs, and showed additive pro-chondrogenesis upon additional TGF-β supplementation (Rothrauff et al., 2017). This may facilitate the development of biological implants with a superior capacity to promote meniscal regeneration than constructs that rely on growth factor stimulation alone (Lee et al., 2014). We used decellularized ECM isolated from young porcine menisci, and assessed its potential for tissue engineering using FPSCs isolated young, healthy porcine joints. The advantage of using animal tissue for ECM extraction is the fact that supply is plentiful and there is a well-established track record of using decellularized porcine tissue clinically for tissue regeneration (Badylak et al., 2009; Lee et al., 2014; Visser et al., 2015; Wolf et al., 2012). Further work is required to confirm that porcine ECM is similarly potent when combined with human cells

isolated from patients with damaged joints. In optimizing ECM functionalised biomaterials for meniscus tissue engineering, it will also be necessary to characterise how different ECM digestion methods will modulate its composition and bioactivity. For example, recent studies have demonstrated that urea-extracted ECMs tended to promote tissue-specific differentiation of MSCs, while pepsin-digested ECM was less effective in this regard (Rothrauff et al., 2017). Identifying the optimal enzymatic or chaotropic agent for ECM solubilisation will be key step in their clinical translation.

3.4. 3D bioprinting of ECM functionalised bioinks mechanically reinforced with PCL

Having demonstrated that ECM functionalized hydrogels can be used to support region specific meniscal tissue engineering, we next sought to evaluate the capacity of such biomaterials to be used as bioinks for 3D bioprinting. To generate printable bioinks, *IN* and *OUT* hydrogels were first pre-crosslinked with 48 mM $CaCl_2$, loaded into the printing column and extruded from a 25 G needle at 1 Bar. A sample print pattern for *OUT* bioinks is shown in Figure 5A. The bioink printability was then evaluated by calculating the filament spreading ratio, which was calculated as 2.87 ± 0.17. Similar results were obtained for the IN bioinks (data not shown).

A major limitation with hydrogels for tissue engineering of load bearing tissues is their poor mechanical properties. The meniscus fibrocartilage equilibrium modulus varies from 0.1 to 1 MPa (Chia and Hull, 2008; Bursac et al., 2009), but most bioinks are significantly softer than such biological materials. We therefore next sought to reinforce the 3D printed bioinks with PCL. By varying fibre diameter, fibre spacing and PCL molecular weight, it is possible to control the mechanical properties of PCL microfibers. Moreover, fibre size and spacing need to be chosen by taking in

consideration that cell-laden hydrogels are deposited between the PCL microfibers. A previous study from our group demonstrated the ability to print in a layer by layer manner, a construct containing both PCL microfibers and hydrogels (Daly et al, 2016). In this study, PCL microfibers (Fig. 5A, right, in white), with a 0.36 ± 0.02 mm thickness and a 1.02 ± 0.05 mm spacing were printed in a layer by layer manner together with the ECM bioink (Fig. 5A, right, in blue). These PCL printing parameters were chosen in an attempt to fabricate constructs with mechanical properties in the range of native meniscus. The equilibrium modulus of cell-laden hydrogels was compared to 3D bioprinted PCL-bioink constructs. As expected, PCL reinforcement led to a greater than 100-fold increase in the stiffness of the printed constructs (Fig. 5B). This value was of a similar order of magnitude to native meniscal tissue mechanical properties. Finally, cell viability within the printed constructs was assessed. FPSCs in constructs with and without PCL reinforcement (Fig. 5C) remained viable (80-90%) 24 h post printing (Fig. 5D). These results suggest that the viability of FPSCs is not affected either by the shear stress caused by the printing process or by the higher temperatures associated with the PCL deposited next to them.

Together our results describe the development of a novel meniscus ECM functionalised bioink that is printable and that can support specific meniscal phenotypes. Future studies will explore the combination of meniscal scanning and bioprinting technology to generate biological constructs resembling the exact anatomic shape of the meniscus. Furthermore, we will utilise multiple-tool biofabrication strategies to spatially deposit different ECM functionalised bioinks inside a reinforcing PCL framework in an attempt to engineer tissues mimicking the spatial complexity of the native meniscus. We are also exploring strategies that will

enable the stable anchoring of bioprinted constructs into the joint, which is another key outstanding challenge related to the clinical translation of engineered meniscal tissues.

4. Conclusions

In this study, alginate hydrogels functionalised with ECM derived from inner and outer regions of the meniscus were able to differently affect cell morphology and to stimulate chondrogenesis and fibrochondrogenesis, respectively, in the absence of exogenously supplied growth factors. Joint derived stem cells encapsulated within the inner ECM bioinks and stimulated with TGFβ3 best supported a chondrogenic phenotype. Cells encapsulated within outer ECM bioinks and stimulated with CTGF best supported a fibroblastic phenotype. Printing PCL in combination with these ECM functionalised bioinks did not negatively impact cell viability. Therefore stem cell laden, ECM functionalised bioinks, combined with PCL micro-fibres for mechanical reinforcement, represents an exciting new approach to tissue engineering functional meniscal grafts.

5. References

Ahn, S, Kim, Y, Lee, H, Kim, G. 2012, A new hybrid scaffold constructed of solid freeform-fabricated PCL struts and collagen struts for bone tissue regeneration: fabrication, mechanical properties, and cellular activity, *Journal of Materials Chemistry,* **22**: 15901.

Almeida, H, Sathy, B, Dudurych, I, Buckley, C, O'Brien, F, Kelly, D. 2017, Anisotropic Shape-Memory Alginate Scaffolds Functionalized with either Type I or Type II Collagen for Cartilage Tissue Engineering, *Tissue Engineering Part A,* **23**:

55–68.

Andia, I, Maffulli, N. 2016, Biological Therapies in Regenerative Sports Medicine. *Sports Medicine*: s40279-01620-z-.

Antony, B, Driban, JB, Price, LL, Lo, GH, Ward, RJ, Nevitt, M, Lynch, J, Eaton, CB, Ding, C, McAlindon, TE. 2016, The relationship between meniscal pathology and osteoarthritis depends on the type of meniscal damage visible on magnetic resonance images: data from the Osteoarthritis Initiative, *Osteoarthritis and Cartilage*: 1–9.

Badylak SF, Freytes, DO, Gilbert, TW. 2009, Extracellular matrix as a biological scaffold material: Structure and function. *Acta Biomater*, **5**: 1-13.

Baek, J, Chen, X, Sovani, S, Jin, S, Grogan, S, D'Lima, D. 2015, Meniscus tissue engineering using a novel combination of electrospun scaffolds and human meniscus cells embedded within an extracellular matrix hydrogel, *Journal of Orthopaedic Research,* **33**: 572–583.

Buckley, C, Vinardell, T, Thorpe, S, Haugh, M, Jones, E, McGonagle, D, Kelly, D, Kelly, DJ. 2010, Functional properties of cartilaginous tissues engineered from infrapatellar fat pad-derived mesenchymal stem cells, *Journal of Biomechanics,* **43**: 920–926.

Bursac, P, Arnoczky, S, York, A. 2009, Dynamic compressive behavior of human meniscus correlates with its extra-cellular matrix composition, *Biorheology,* **46**: 227–237.

Carroll, SF, Buckley, CT, Kelly, DJ. 2014, Cyclic hydrostatic pressure promotes a stable cartilage phenotype and enhances the functional development of cartilaginous grafts engineered using multipotent stromal cells isolated from bone marrow and infrapatellar fat pad, *Journal of Biomechanics,* **47**: 2115–21.

Chia, HN, Hull, ML. 2008, Compressive moduli of the human medial meniscus in the

axial and radial directions at equilibrium and at a physiological strain rate, *Journal of Orthopaedic Research,* **26**: 951–956.

Daly, A, Critchley, S, Rencsok, E, Kelly, D. 2016, A comparison of different bioinks for 3D bioprinting of fibrocartilage and hyaline cartilage, *Biofabrication,* **8**: 45002.

Fisher, M, Henning, E, Söegaard, N, Bostrom, M, Esterhai, J, Mauck, R. 2017, Engineering meniscus structure and function via multi-layered mesenchymal stem cell-seeded nanofibrous scaffolds, *Journal of Biomechanics,* **48**: 1412–1419.

Fisher, M, Henning, E, Söegaard, N, Esterhai, J, Mauck, R. 2013, Organized nanofibrous scaffolds that mimic the macroscopic and microscopic architecture of the knee meniscus, *Acta Biomaterialia,* **9**: 4496–4504.

Hong, S, Sycks, D, Chan, H, Lin, S, Lopez, G, Guilak, F, Leong, K, Zhao, X. 2015, 3D Printing of Highly Stretchable and Tough Hydrogels into Complex, Cellularized Structures, *Advanced Materials,* **27**: 4035–4040.

Lee, C, Moioli, E, Mao, J. 2006, Fibroblastic differentiation of human mesenchymal stem cells using connective tissue growth factor. *CConf Proc IEEE Eng Med Biol Soc.,* **1**: 775–8.

Lee, C, Shah, B, Moioli, E, Mao, J. 2010, CTGF directs fibroblast differentiation from human mesenchymal stem/stromal cells and defines connective tissue healing in a rodent injury model, *The Journal of clinical investigation,* **120**: 3340–9.

Lee, H, Koh, W, Lee, C, Rodeo, S, Fortier, L, Lu, C, Erisken, C, Mao, J. 2014, Protein-releasing polymeric scaffolds induce fibrochondrocytic differentiation of endogenous cells for knee meniscus regeneration in sheep, *Sci Transl Med,* **6**: 1–12.

Luo, L, O'Reilly, A, Thorpe, S, Buckley, C, Kelly, D. 2016, Engineering zonal cartilaginous tissue by modulating oxygen levels and mechanical cues through the depth of infrapatellar fat pad stem cell laden hydrogels, *J Tissue Eng Regen Med*:

May 3.

Makris, A, Hadidi, P, Athanasiou, K. 2011, The knee meniscus: structure-function, pathophysiology, current repair techniques, and prospects for regeneration, *Biomaterials,* **32**: 7411–7431.

Markstedt, K, Mantas, A, Tournier, I, Martínez, ÁH, Hägg, D, Gatenholm, P. 2015, 3D bioprinting human chondrocytes with nanocellulose-alginate bioink for cartilage tissue engineering applications. *Biomacromolecules,* **16:** 1489–1496.

Di Matteo, B, Perdisa, F, Gostynska, N, Kon, E, Filardo, G, Marcacci, M. 2015, Meniscal Scaffolds - Preclinical Evidence to Support their Use: A Systematic Review, *The open orthopaedics journal,* **9**: 143–56.

Mesallati, T, Sheehy, E, Vinardell, T, Buckley, C, Kelly, D. 2015, Tissue engineering scaled-up, anatomically shaped osteochondral constructs for joint resurfacing, *Eur Cell Mater,* **30**: 163–186.

Moioli, E, Mao, J. 2006, Chondrogenesis of Mesenchymal Stem Cells by Controlled Delivery of Transforming Growth Factor-beta3, *Conf Proc IEEE Eng Med Biol Soc.,* **1**: 2647–2650.

Moran, C, Busilacchi, A, Lee, C, Athanasiou, K, Verdonk, P. 2015, Biological Augmentation and Tissue Engineering Approaches in Meniscus Surgery, *Arthroscopy* **31**: 944–55.

OECD/EU. 2016, *Health at a Glance: Europe 2016- State of Health in the EU Cycle*, OECD Publishing.

Olvera, D, Daly, A, Kelly, DJ. 2015, Mechanical Testing of Cartilage Constructs, *Methods Mol Biol*, **1340**: 279–287.

Park, KH, Na, K. 2008, Effect of growth factors on chondrogenic differentiation of rabbit mesenchymal cells embedded in injectable hydrogels, *Journal of bioscience*

and bioengineering, **106**: 74–79.

Parker, BR, Hurwitz, S, Spang, J, Creighton, R, Kamath, G. 2016, Surgical Trends in the Treatment of Meniscal Tears: Analysis of Data From the American Board of Orthopaedic Surgery Certification Examination Database, *Am J Sports Med.,* **44**: 1717–23.

Pati, F, Jang, J, Ha, D, Kim, S, Rhie, J, Shim, J, Kim, D, Cho, D. 2014, Printing three-dimensional tissue analogues with decellularized extracellular matrix bioink, *Nature Communications,* **5**: 1–11.

Rothrauff, B, Yang, G, Tuan R. 2017, Tissue-specific bioactivity of soluble tendon-derived and cartilage-derived extracellular matrices on adult mesenchymal stem cells, *Stem Cell Res Ther*, **8**: 133.

Rothrauff, B, Shimomura, K, Gottardi, R, Peter, G, Tuan, R. 2016, Anatomical region-dependent enhancement of 3-dimensional chondrogenic differentiation of human mesenchymal stem cells by soluble meniscus extracellular matrix, *Acta Biomaterialia,* **49**: 140–151.

Scotti, C, Hirschmann, M, Antinolfi, P, Martin, I, Peretti, G. 2013, Meniscus repair and regeneration: review on current methods and research potential, *Eur Cell Mater,* **26**: 150–170.

Shimomura, K, Rothrauff, B, Tuan, R. 2016, Region-Specific Effect of the Decellularized Meniscus Extracellular Matrix on Mesenchymal Stem Cell – Based Meniscus Tissue Engineering, *Am J Sports Med,* **45**: 604–611.

Skardal, A, Atala, A. 2015, Biomaterials for Integration with 3-D Bioprinting, *Annals of Biomedical Engineering*, **43**: 730–746.

Steadman, JR, Rodkey, WG. 2017, Tissue-Engineered Collagen Meniscus Implants: 5- to 6-Year Feasibility Study Results, *Arthroscopy,* **21**: 515–525.

Van der Bracht, H, Verdonk, R, Verbruggen, D, Elewaut, D, Verdonk, P. 2007. Stem Cell-Based Meniscus Tissue Engineering. *In: Topics in tissue engineering,* R Reis & E Chiellini, p 1–13.

Vinardell, T, Sheehy, E, Buckley, C, Kelly, D. 2012, Phenotypic Stability of Cartilaginous Tissues Engineered from Different Stem Cell Sources, *Tissue Engineering Part A,* **18**: 1161–1170.

Visser, J, Levett, P, Moller, N, Besems, J, Boere, K, van Rijen, M, de Grauw, J, Dhert, W, van Weeren, P, Malda, J. 2015, Crosslinkable Hydrogels Derived from Cartilage, Meniscus, and Tendon Tissue, *Tissue Engineering Part A,* **21**: 1195–206.

Vrancken, A, Buma, P, Van Tienen, T. 2013, Synthetic meniscus replacement: A review, *International Orthopaedics,* **37**: 291–299.

Wolf, MT, Daly, KA, Brennan-pierce, EP, Johnson, SA, Carruthers, C, Amore, AD, Nagarkar, SP, Sachin, S, Badylak, SF. 2012, A hydrogel derived from decellularized dermal extracellular matrix. *Biomaterials*, **33**: 7028-7038.

Wu, J, Ding, Q, Dutta, A, Wang, Y, Huang, Y, Weng, H, Tang, L, Hong, Y. 2015, An injectable extracellular matrix derived hydrogel for meniscus repair and regeneration, *Acta Biomaterialia,* **16**: 49–59.

Yang, F, Tadepalli, V, Wiley, BJ. 2017, 3D Printing of a Double Network Hydrogel with a Compression Strength and Elastic Modulus Greater than those of Cartilage. *ACS Biomaterials Science and Engineering,* **3**: 863-869.

Yu, H, Adesida, A, Jomha, N. 2015, Meniscus repair using mesenchymal stem cells – a comprehensive review, *Stem cell Res Ther,* **6**: 86.

Figure Legends

Fig. 1: Meniscus ECM isolation and characterization. Porcine meniscus was isolated, divided into two parts (outer and inner regions as defined by their consistency and appearance), pepsin digested and freeze dried (A). The obtained inner and outer ECM were resolubilized in 0.02% acetic acid, stained for collagen type I (Col.I) and collagen type II (Col.II), and compared to commercially available type I collagen (Comm. Col.I) and commercial type II collagen (Comm. Col.II) (B). Nuclei were counterstained in blue (DAPI) to ensure absence of DNA. Scale bars: 100 μm.

Fig. 2: ECM effect on FPSC phenotype and differentiation.

Cells were encapsulated in alginate hydrogels (5 x 3 mm) containing either inner ECM (*IN*) or outer ECM (*OUT*). FPSC in alginate only gels (*ALG*) were used as a control. All groups were kept in culture for 21 days. Cell morphology was detected by immunofluorescence staining of F-actin through Phalloidin-TRITC (A, red) (Scale bar: 100 μm). Nuclei were counterstained in blue (DAPI) (A). Immunohistochemical analysis to evaluate Collagen type I (B) and type II (C) deposition, and quantified by RT-PCR (C and E, respectively) (Scale bar: 200 μm). Aldehyde fuchsin/alcian blue for sGAG synthesis (F) and biochemical analysis for sGAG quantification (sGAG/DNA) (G) (n=5, ANOVA, Mean±SD). Scale bar: 100 μm. * $P<0.05$, ** $P<0.001$ and *** $P<0.0001$.

Fig. 3: The effect of ECM and exogenous growth factors on FPSC morphology and matrix synthesis

FPSCs were encapsulated into alginate only (*ALG*) or inner ECM (*IN*) or outer ECM

(*OUT*) functionalized alginate and then cultured in media containing either CTGF or TGFβ3 for 21 days. ACTIN (red) and DAPI (staining) for cell morphology evaluation in all groups (A) (Scale bar: 250 μm). Biochemical analysis for sGAG content in CTGF (B) and TGFβ3 (D) treated constructs (n=5, ANOVA, Mean±SD); * $P<0.05$ and *** $P<0.0001$. Aldehyde fuchsin/alcian blue for sGAG detection in cells cultured in CTGF (C) and TGFβ3 (E) supplemented media. Scale bar: 100 μm.

Fig. 4: The effect of ECM and exogenous growth factors on FPSC phenotype and collagen synthesis Immunohistochemical analysis of FPSC laden hydrogels following 21 days culture in either CTGF (A) or TGFβ3 (B) supplemented media. Collagen type I (Col.I), collagen type II (Col.II), Sox9, ACAN and TNC gene expression was quantified by RT-PCR analysis (C-G). The expression of all genes except Col.II was normalised to that of FPSCs maintained in monolayer culture in standard culture dishes and standard expansion media (Ctrl). As FPSCs in monolayer culture did not express type II collagen, the expression of this gene in each group was normalised to that of ALG gels stimulated with CTGF. * $P<0.05$, ** $P<0.001$ and *** $P<0.0001$. Scale bar: 100 μm.

Fig. 5: 3D Bioprinting of ECM functionalised hydrogels reinforced with PCL Printed hydrogel pattern using ECM-alginate bioinks (A, left) and bioink plus PCL reinforcement (A, right) (Scale bars: 1 mm). Equilibrium modulus of all printed hydrogels compared to PCL reinforced constructs (B) (n=3, ANOVA, $p<0.05$, Mean±SD). *** versus Bioink + PCL. Representative live dead staining of cells printed with (C, right) or without (C, left) PCL incorporation in the construct (Scale bars: 250 μm). Quantification of cell viability (D) (n=4, ANOVA, Mean±SD).

Fig. 1

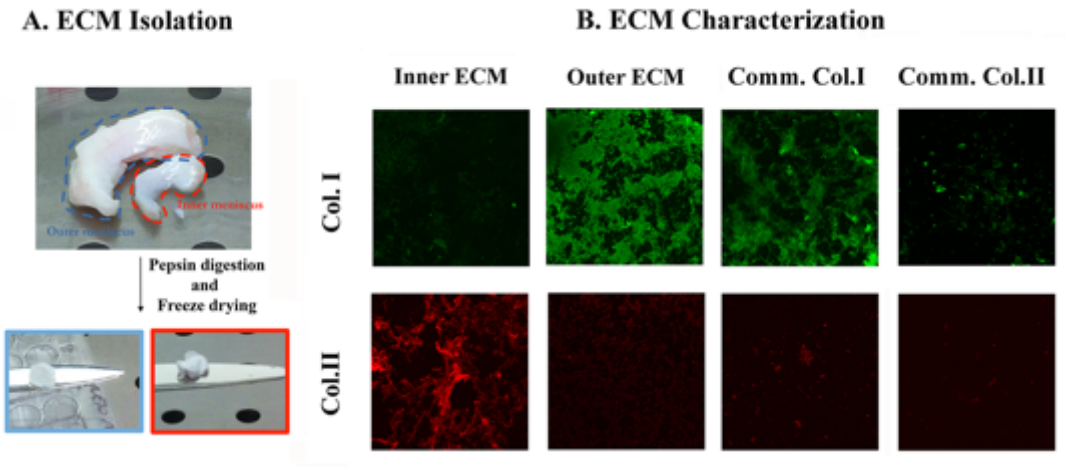
A. ECM Isolation
B. ECM Characterization
Inner ECM
Outer ECM
Comm. Col.I
Comm. Col.II
Col. I
Col.II
Pepsin digestion
and
Freeze drying

Fig. 2

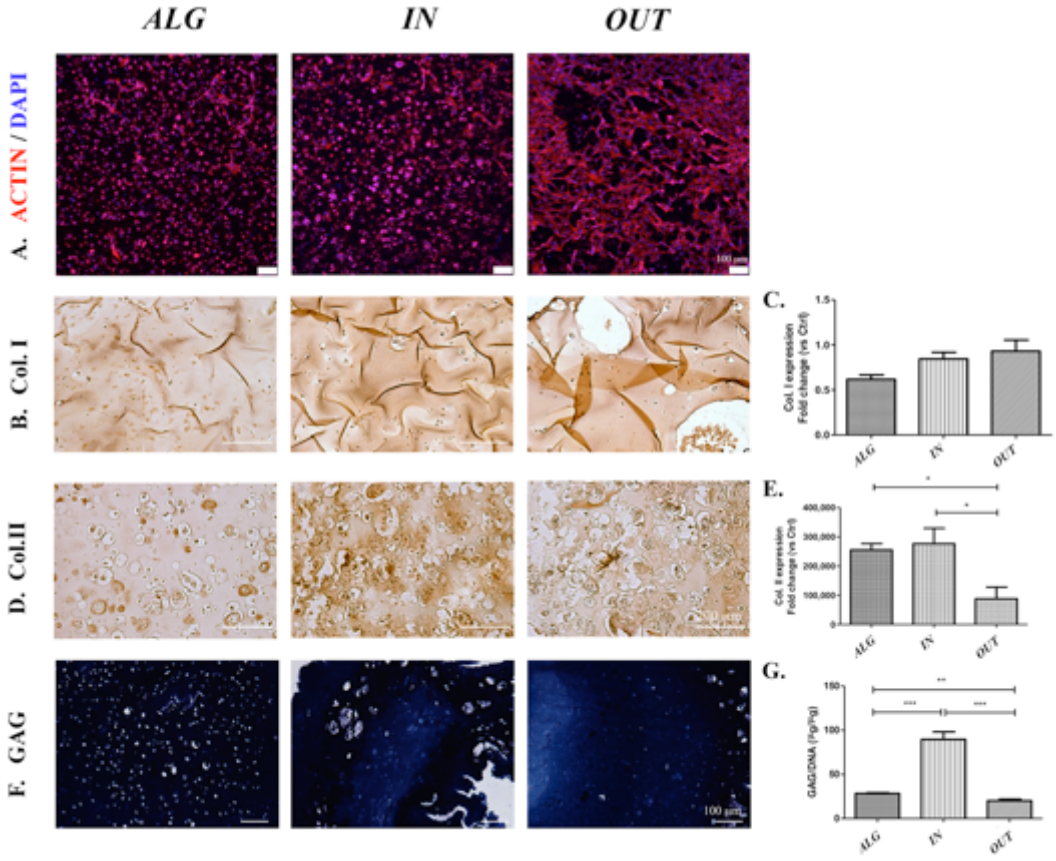
ALG
IN
OUT
A. ACTIN / DAPI
B. Col. I
D. Col.II
F. GAG
C.
E.
G.

Fig. 3

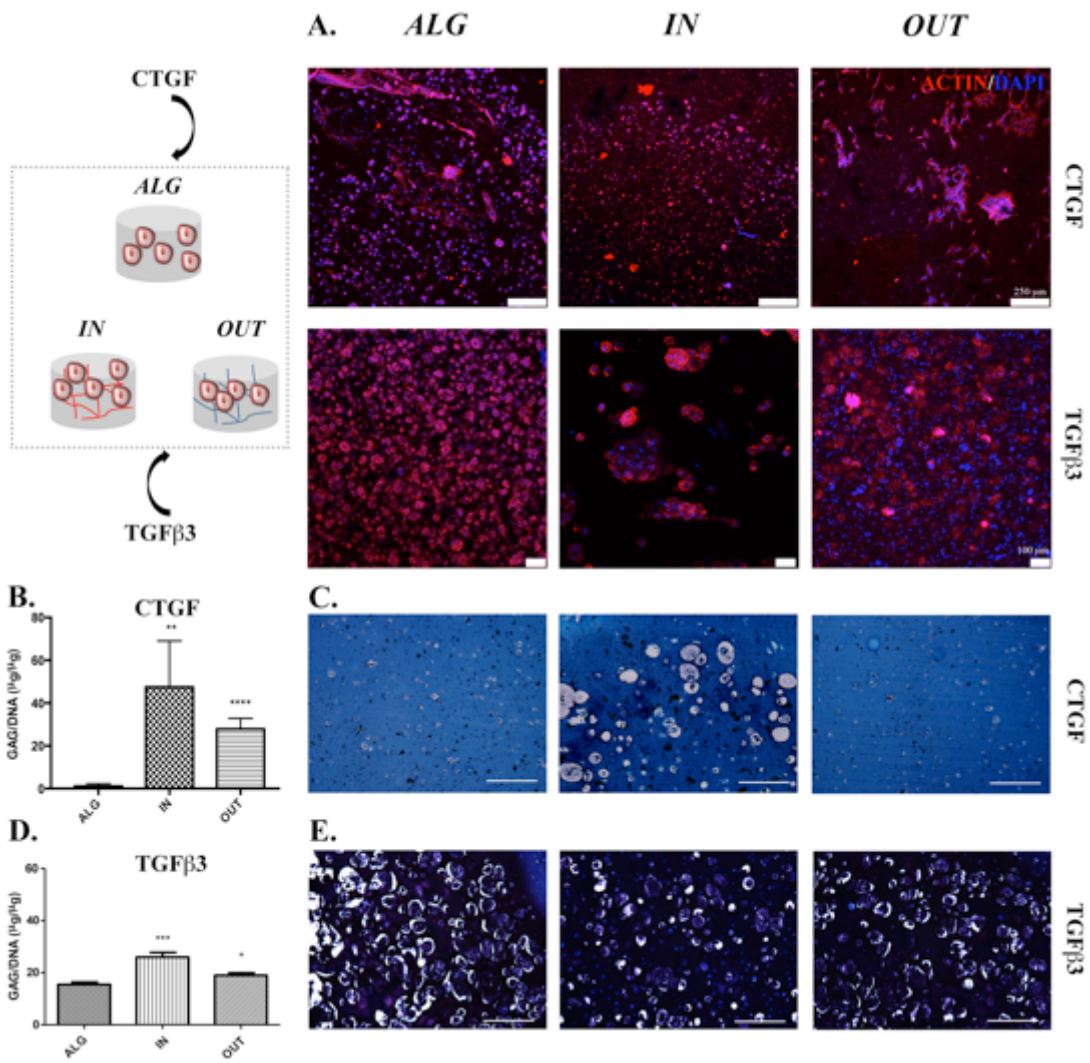
A.
ALG
IN
OUT
ACTIN/DAPI
CTGF
TGFβ3
CTGF
TGFβ3
B.
CTGF
GAG/DNA (µg/µg)
ALG
IN
OUT
C.
CTGF
D.
TGFβ3
GAG/DNA (µg/µg)
ALG
IN
OUT
E.
TGFβ3

Fig. 4

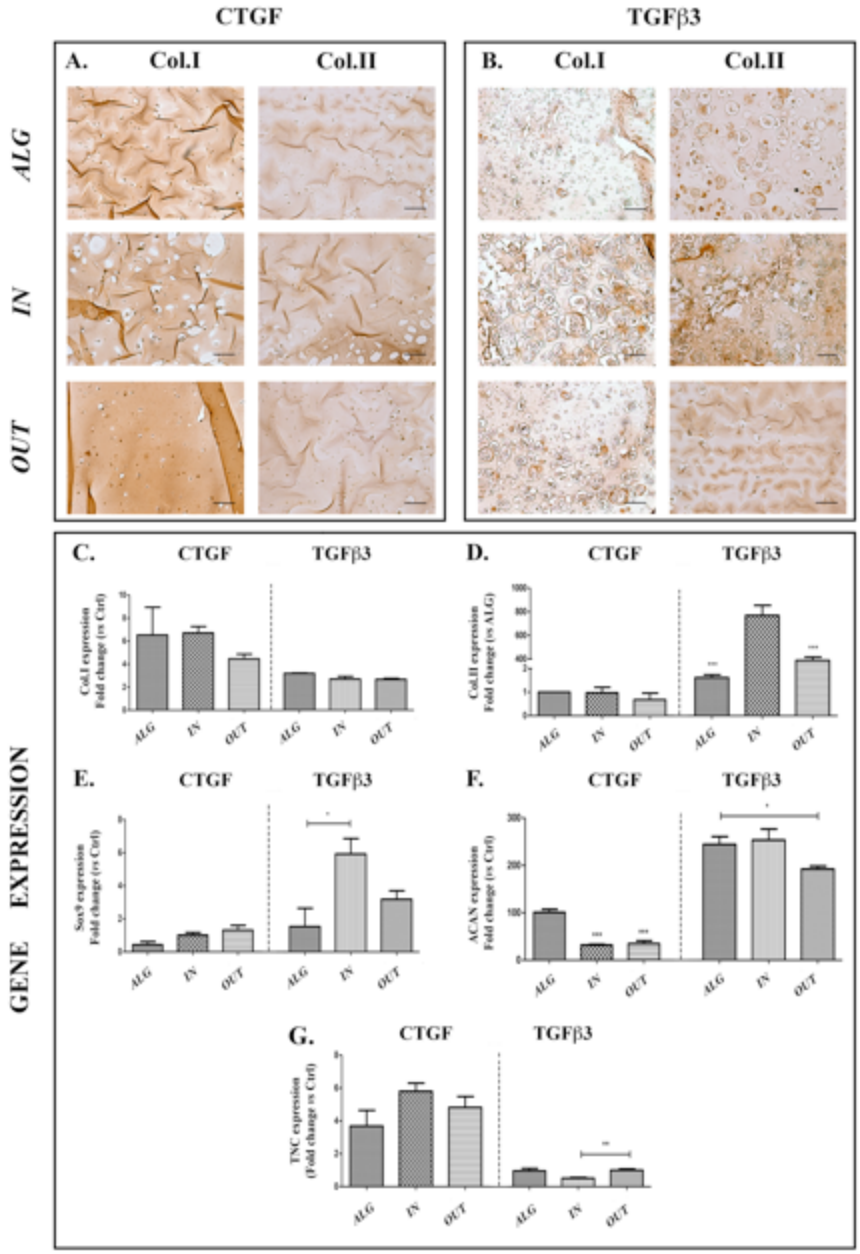
CTGF
TGFβ3
A.
Col.I
Col.II
B.
Col.I
Col.II
ALG
IN
OUT
GENE EXPRESSION
C.
CTGF
TGFβ3
Col.I expression
Fold change (vs Ctrl)
D.
CTGF
TGFβ3
Col.II expression
Fold change (vs ALG)
E.
CTGF
TGFβ3
Sox9 expression
Fold change (vs Ctrl)
F.
CTGF
TGFβ3
ACAN expression
Fold change (vs Ctrl)
G.
CTGF
TGFβ3
TNC expression
(Fold change vs Ctrl)
ALG
IN
OUT

Fig. 5

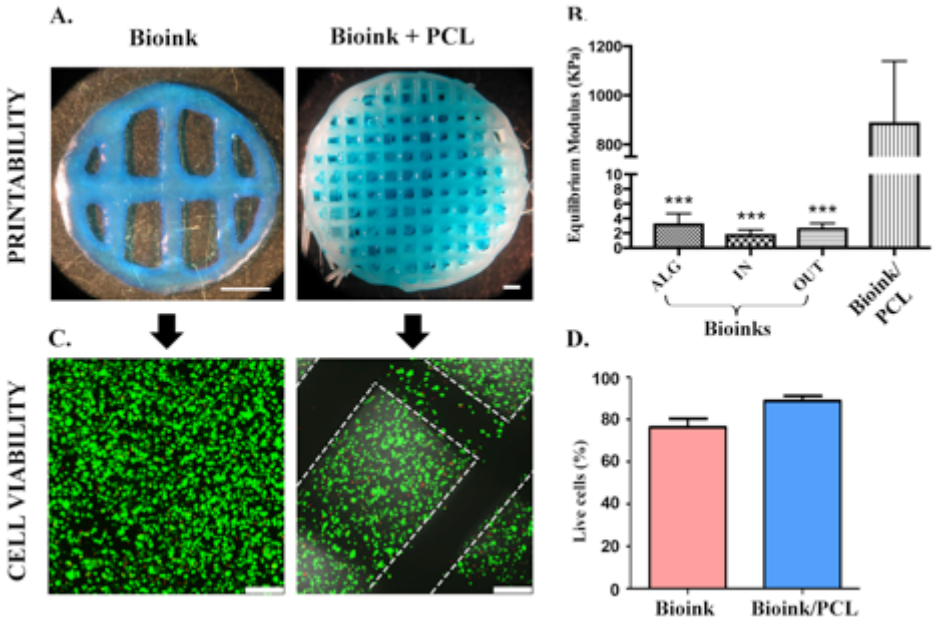
A.
Bioink
Bioink + PCL
PRINTABILITY
B.
Equilibrium Modulus (KPa)
1200
1000
800
10
8
6
4
2
0
***
***
***
ALG
IN
OUT
Bioink/
PCL
Bioinks
C.
CELL VIABILITY
D.
Live cells (%)
100
80
60
40
20
0
Bioink
Bioink/PCL